Synthesis of ZnO nanoparticles at room temperature with enhanced ultra-violet photoluminescence

Subhamay Pramanik[1], #, Sumit Mukherjee[1], Sandip Das[1] and Probodh K. Kuiri[1],*

1Department of Physics, Sidho-Kanho-Birsha University, Purulia, West Bengal, 723104, India

Abstract

ZnO nanoparticles (NPs) have attracted a lot of attention due to the possibility of their applications in different fields including optoelectronics, photonics, biosensing, catalytic, etc. Most of the applications require devices made of good quality of NPs. However, synthesis of device grade NPs is always challenging. Here, improvement of crystalline quality of the ZnO NPs has been demonstrated with a very simple procedure. ZnO NPs of average crystallite size of ~11.5 nm with optical band gap of ~3.44 eV have been synthesized in room temperature following the co-precipitation method by either varying the concentration of KOH or time of synthesis. For both the cases, change in average size of NPs has not been found to change significantly. This is mainly because the required heat energy to grow the size has not been provided externally. However, the increase of concentration of KOH or time of preparation has been found to improve the quality of the ZnO crystallites. The improvement of crystalline quality has been argued as due to the availability of enough KOH or the time to repair the defects on the surface of the NPs. Improvement of crystalline quality has been found to result in an enhancement of intensity of the ultra-violet (UV) photoluminescence (PL) emission band over the visible PL emission band of ZnO. The defect mediated visible PL emission is always considered as loss. The enhancement is ~2-*fold.* Such large enhancement can be utilized for the fabrication of optoelectronic devices and others based on ZnO NPs synthesized at room temperature.

Keywords: ZnO nanoparticle, Synthesis, Room temperature, Photoluminescence, Enhancement

1. Introduction

Zinc oxide (ZnO) nanostructures have attracted a lot of attention, recently, due to their unique properties compared to its bulk counterpart [1,2,3]. Due to large exciton binding energy (60 meV at room temperature) excitonic recombination process can take place with possibility of optically pump lasing even at room temperature [4]. After the experimental demonstrations of light emitting diode in blue-green region and lasing action using ZnO nanostructures, a lot of studies were carried out to make use of it for optoelectronic applications covering both visible and ultra-violet (UV) regions. Observation of two photoluminescence (PL) emissions bands in UV and visible regions is considered as one of the prominent optical properties of ZnO nanoparticles (NPs) [5]. The origin of the UV and visible emissions are the radiative transitions of electrons from the conduction band (i.e. the near band edge emission) and from the various defect states (on the NP surface), respectively, to the valence band [5]. The defect states of ZnO NPs trap carriers and result in low PL efficiency [6]. Such reduction of PL efficiency makes ZnO NPs unsuitable for many useful practical applications. Hence for practical applications of the ZnO NPs, minimization of defect mediated emission is desirable. In a recent study, we have shown that nearly defect-free PL emission is possible by synthesizing ZnO NPs using co-precipitation method with a proper choice of precursor concentration [7]. Also simultaneous reduction of defect emission and enhancement of UV emission has been demonstrated for nanocrystalline ZnO films grown on Ag NPs embedded in silica glass [8]. In the present study, we show a significant reduction of visible PL emission of ZnO NPs synthesized at room temperature using co-precipitation method by controlling the synthesis parameter *viz.* increasing the concentration of KOH or time of synthesis. The major advantage of the present study is that the synthesis of ZnO NPs does not require heat treatment usually needs for the precipitation of the NPs. It is worth mention that the co-precipitation method has certain advantages over the other methods. For example, this method can produce high quality crystalline materials through an energy efficient route that allows wide area growth. In fact, by changing the preparation parameters (time, temperature, pH value, pressure, doping concentration, etc.), size as well as morphology of the NPs can be tuned [2,5,9,10,11,12].

2. Experiments

In this present study, two sets of samples were prepared. In one set, the time of synthesis was kept

#Electronic mail: subhaphys90@gmail.com
probodh@skbu.ac.in

fixed to 40 days and concentrations of KOH were varied to values of 0.5 M, 0.75 M, and 1.0 M. In second set, the concentration of KOH was kept fixed to 1.0 M and the time of was varied to values of 10 days, 20 days, 40 days, and 60 days. In this typical procedure ZnO NPs have been synthesized using room temperature co-precipitation method. Zinc acetate dihydrate $((Zn(Ac)_2 \cdot 2H_2O))$ and KOH are used as precursors materials. For the first set of samples, 0.5 M of $Zn(Ac)_2 \cdot 2H_2O$ was dissolved in 300 ml ethanol stirred for 30 min for homogeneous solution and then divided it into three equal parts i.e. 100 ml each. Another solution of KOH in 50 ml ethanol was prepared by varying concentrations of 0.5 M, 0.75M, and 1 M. Then the KOH solutions were mixed in $Zn(Ac)_2 \cdot 2H_2O$ solutions drop-wise and stirred for 2 hours at room temperature. The as-synthesized samples were sealed and stored for 40 days. After 40 days the prepared samples were cleaned by centrifugation at 4000 rpm for 4 min using ethanol and stored for further characterizations. Another set of ZnO NPs was prepared using above mentioned methods by varying the time of preparation i.e. 10 days, 20 days, 40 days, and 60 days for the fixed concentration of KOH viz. 1 M.

In the present report, we have used KOH as a precipitation agent instead of NaOH or LiOH. This is because of the higher ionic radius of the K^+ ion (152 pm), compare to Na^+ (92 pm) or Li^+ (116 pm), due to large ionic radius the possibility of penetration into the ZnO host during the growth becomes very poor [11]. Furthermore, the dissociation constant (K_D) of KOH is the largest relative to NaOH and LiOH $(K_D^{LiOH} < K_D^{NaOH} < K_D^{KOH})$ and hence, more OH^- ions can be supplied by KOH under the same experimental conditions [11, 19]. As a result, with KOH, conversion of ZnO from the zinc acetate di-hydrate becomes faster. Due to these advantages KOH has been chosen as the precipitating agent in the present article.

All the samples were characterized using X-ray diffractometer (PROTO AXRD) with Cu K_α radiation (λ=0.15406 nm) for scan angle (2θ) in the range of $25^0 - 75^0$. Fourier transformed infrared (FTIR) spectroscopy measurements were carried out on a few of the selected samples using the Perkin Elmer Spectrum model L1600300 machine in the wavenumber range of $450 - 4000$ cm^{-1}. PL measurements were carried out using CARY Eclipse (Agilent) with excitation wavelengths of 330 nm, 340 nm, and 350 nm. The optical absorption (OA) measurements were carried out using a JASCO V-630 double beam spectrophotometer. Ethanol has been used as solvent for PL and OA measurements. All the measurements were carried out at room temperature.

3. Results and discussion

Figure 1 shows the X-ray diffraction (XRD) spectra of ZnO NPs synthesized for 40 days using different concentrations viz 0.5 M, 0.75 M, and 1.0 M of KOH. For 0.5 M of KOH, peaks at around 31.89^0, 34.47^0, 36.29^0, 46.76^0, 56.74^0, 62.95^0, and 67.90^0 in the XRD spectrum are seen. These peaks are identified as (100), (002), (101), (102), (110), (103), and (112) crystalline planes of wurtzite ZnO crystals [5]. These are marked in the figure. The first three peaks [corresponding to planes of (100), (002), and (101)] are more intense than the other peaks. This indicates that the ZnO crystals have grown preferentially in these directions. Such growth is due to the lower free energies of crystalline ZnO having planes of (100), (002), and (101) compared to those of the other planes. Non observation of impurity phases in the diffraction peaks confirm that the ZnO NPs are of high purity. Similar peaks in the XRD spectra are also seen in other two samples (with 0.75 M and 1.0 M of KOH) and are shown in the same figure. An additional peak at $\sim 69.13^0$ is seen to appear for the sample with 0.75 M of KOH. This peak is clearly visible for the sample with 1.0 M of KOH. This peak is due to the (201) crystalline plane of wurtzite ZnO crystal [5]. One can see in Figure 1 that the intensity of each of the XRD peak increases with increase in KOH concentration. This is due to the growth of more number of ZnO NPs with increase in concentration of KOH.
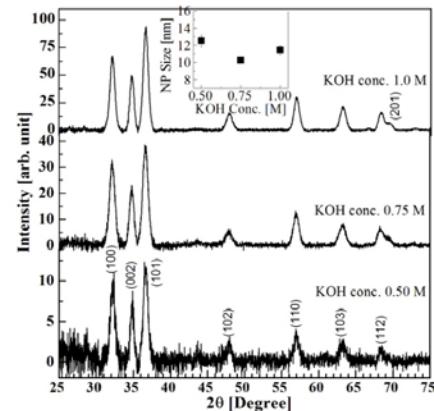

Figure 1: XRD spectra of ZnO NPs prepared for 40 days for different concentrations of KOH. Inset: Variation of average size of NP with concentration of KOH.

Using the XRD data, the average size of the crystallites, *D*, can be estimated using Scherrer formula [5]

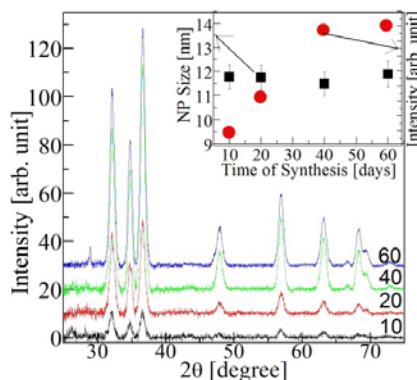$$D = \frac{0.94\lambda}{\beta \cos\theta}, \qquad (1)$$

where, λ is the wavelength of X-ray radiation (0.154 nm), β is the full width at half maximum (FWHM) in radian of XRD peak, and θ is the XRD peak

position. For estimation of D, we have used the most intense XRD peak [i.e., peak corresponding to the plane of (101)] for each of the XRD spectra. Measured β contains the instrumental broadening also. Hence it is essential to eliminate the instrumental broadening from β to estimate the true sizes of ZnO crystallites from the XRD measurements. For this purpose, we have used the following equation to get correct value of FWHM, β_{cor},

$$\beta_{cor} = \sqrt{(\beta_m)^2 - (\beta_i)^2} \qquad (2)$$

where, β_m is the measured FWHM and β_i is the instrumental broadening (FWHM) which is equal to 0.103^0 for the XRD used for characterizations of the samples. The estimated average size of the crystallites (or NPs) are about 12.5 nm, 10.3 nm, and 11.4 nm for KOH concentrations of 0.5 M, 0.75 M, and 1.0 M, respectively. Inset of Figure 1 shows the variation of average size of NPs with concentration of KOH. These sizes are within 2 nm of difference and almost fall within the error in the measurement. Thus the average sizes of the ZnO NPs are nearly same for the samples with different concentrations of KOH. The XRD analysis confirmed that the ZnO NPs were synthesized at room temperature using chemical precipitation method for all the three concentrations of KOH used. The number of ZnO NPs was found to increase with increase in concentration of KOH as the intensity of each of the XRD peak increases with increase in concentration of KOH. Recently Cao et al and other research groups also reported similar type of results, they control the size and shape of the ZnO NPs by varying concentration of NaOH and time of preparation [20-22].

As mentioned above (in Experiments), the ZnO NPs were also synthesized for different times viz 10 days, 20 days, 40 days, and 60 days while keeping the KOH concentration of 1 M fixed. The XRD spectra for the ZnO NPs synthesized using 1 M of KOH for different times (10 days – 60 days) are shown in Figure 2. For clarity, the XRD spectra corresponding to 20 days, 40 days, and 60 days are shifted vertically upward. Again, all the XRD peaks as observed in Figure 1 are also seen in Figure 2:

XRD spectra of ZnO NPs prepared using KOH concentration of 1 M for different time (days).

The unit of 10, 20, 40 and 60 against each of the XRD spectra is in days. The XRD spectra corresponding to 20, 40, and 60 days have been shifted vertically upward for clarity. Inset: variations of average size of NP and intensity of (101) XRD peak as a function of synthesis time.

Figure 2 for all the four samples prepared for different time. Intensities of the XRD peaks for the samples corresponding to time of synthesis of 10 – 40 days are found to increase significantly with increase in time. Such increase in intensity indicates synthesis of more number of ZnO NPs with increase in time. Variation of intensity of (101) peak with time of synthesis is shown in inset of Figure 2 (filled circles). Peak intensity increases linearly with time of synthesis up to 40 days. Beyond 40 days, the intensity does not increase anymore. Although, the number of ZnO NPs increases linearly up to 40 days, number of NPs does not increase beyond 40 days. We have also estimated the average sizes of the NPs using eq, (1) considering the XRD peak corresponding to the plane (101). The average sizes of the ZnO NPs are found to be about 11.8 nm, 11.7 nm, 11.5 nm, and 11.9 nm for the time of synthesis of 10 days, 20 days, 40 days, and 60 days, respectively. The variation of the average size of NPs with the time of synthesis is also shown in the inset of Figure 2 (filled squares). It is important to mention that the average sizes of NPs do not change with the time of synthesis even with a large time (50 days) gap. This is due to mainly the nonavailability of sufficient thermal energy to grow the ZnO NPs with time as the synthesis was carried out at room temperature. For the growth of ZnO NPs with the increase in time, sufficient thermal energy is required [5]. In an earlier study, we have shown that ZnO NPs can grow significantly with an increase in time when synthesized at atemperature of ~64 °C [5].
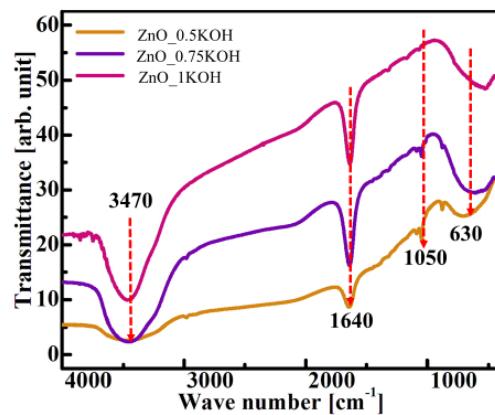

Figure 3. shows the FTIR spectra of ZnO NPs for different KOH concentrations viz 0.5 M, 0.75 M, and 1.0 M.

The spectra show several dips for various vibrational modes. The dip at 3470 cm^{-1} originates OH starching modes of residual alcohols [13]. The dip at 1800 cm^{-1} and 1000 cm^{-1} is ascribed as C=C, C-H$_2$, CH, etc bonds [14]. The broad dip centered around 630 cm^{-1} is assigned as Zn-O starching mode [15]. This absorption band is seen for all three samples confirming the successful formation of ZnO.

Figure 3: FTIR spectra of the ZnO NPs synthesized for a fixed time of 40 days with varying concentrations of KOH. The values 0.50 M, 0.75 M, and 1.00 M correspond to the KOH concentration.

Both the XRD and the FTIR studies have confirmed the synthesis of ZnO particles at room temperature. As the average size of the ZnO particles is about 11.5 nm, confinement effects within the NPs are expected [5,7]. Using the suitable theory based on quantum confinement effects, one can estimate the bandgap of ZnO NPs using the measured size of NPs from OA spectrum(The nature of the OA spectrum is excitonic). Two theories viz Brus theory [16] and effective mass approximation (EMA) model [2] are generally used to calculate the optical band gap of semiconductor NPs. The Brus theory is used for strong confinement region whereas EMA model is used for weak confinement region. When the size of NP is equal to or smaller than the Bohr exciton radius, the NPs show strong confinement effects. On the other hand, when the size of NP is larger than the Bohr exciton radius, the NPs show weak confinement effects. As the Bohr exciton radius of ZnO is 2.87 nm [17] and the estimated average size of NP is ~11.5 nm, the EMA model can be used for estimation of the optical bandgap of the as-synthesized ZnO NPs. In the EMA model, the effective bandgap energy, E_g^{eff}, is given by [2]

$$E_g^{\text{eff}} = E_g + \frac{h^2}{8\mu R^2}, \qquad (3)$$

where E_g is the bulk bandgap energy, R is the particle radius, h is the Planck constant, and μ is the reduced effective mass with $\frac{1}{\mu} = \frac{1}{m_e^*} + \frac{1}{m_h^*}$; m_e^* and m_h^* being the electron and hole effective masses, respectively. For ZnO, E_g = 3.37 eV, m_e^* = $0.24 m_0$, and m_h^* = $0.45 m_0$; m_0 being the rest mass of the electron [18]. The variation of effective bandgap with a diameter of ZnO NP calculated using eq. (3) is shown in Figure 4. The bandgap increases with a decrease in the size of NP. Now using the value of the size of NP (11.5 nm for the present study) on the curve of Figure 4, one can estimate the (effective) bandgap of ZnO NP. The estimated bandgap of the as-synthesized ZnO NPs is 3.44 eV.
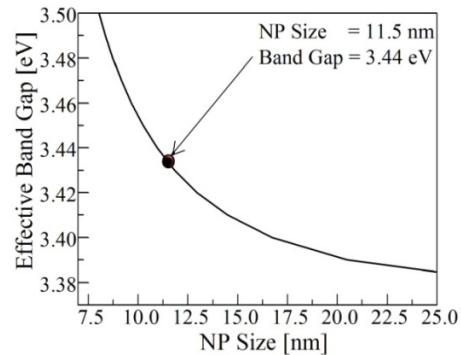

Figure 4: Variation of the effective bandgap of ZnO NPs as a function of NP size according to EMA model. The filled circle is the measured average size of ZnO NP corresponding to bandgap of 3.44 eV.

Figure 5(a) shows the PL spectra of ZnO NPs synthesized for 40 days with different concentrations of KOH. The PL spectra were measured for excitation of 330 nm of wavelength. Mainly two PL emission bands are seen: one narrow band in the UV region and the other broadband in the visible region. For comparison, all the spectra have been normalized to unity at the UV peak. The intensity of the UV band is relatively stronger than that of the visible band for all the samples. This is indicative of the synthesis of good crystalline ZnO NPs. The UV peak is due to the band-to-band transition in ZnO NPs [5,7]. The width of this peak is seen to decrease with an increase in the concentration of KOH [inset of Figure 5(a)]. This decrease is faster from 0. 5 M to 0.75 M and is slower from 0.75 M to 1.0 M. A reduction of FWHM of the UV PL emission peak is indicative of the formation of improved crystallites quality of ZnO NPs [16]. Thus the crystal quality of ZnO NPs is found to improve significantly for KOH concentration of 0.75 M. Again the crystal quality of ZnO NPs further improves for 1 M of KOH. Although the ZnO NPs are formed for all the concentrations of KOH, the use of 1 M (highest concentration used) of KOH resulted in the synthesis of good quality ZnO NPs. The ZnO NPs synthesized for lower concentrations of KOH are having a lot of defects in them. Lower is the concentration of KOH higher are the defects in ZnO NPs. Usually, the defects reside near the surface of ZnO NPs [5,7,8]. The observed visible emissions are the direct consequences of several defect-mediated emissions of ZnO NPs [5,7,8].
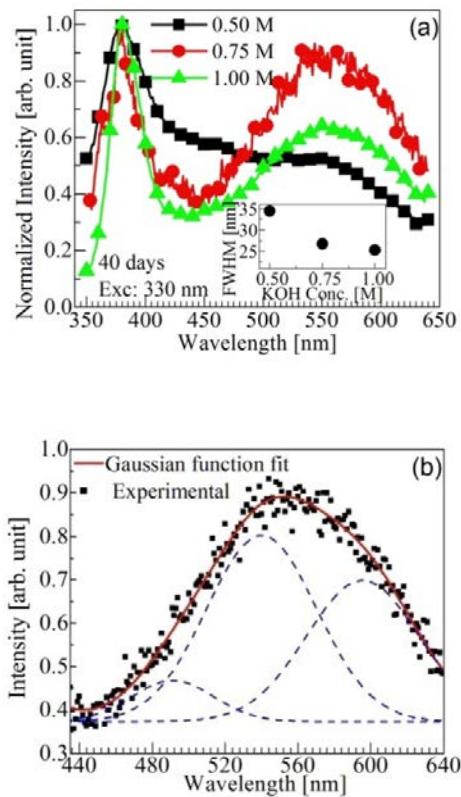
Figure 5: (a) PL spectra of ZnO NPs synthesized for 40 days for different concentrations of KOH. Inset: Variation of FWHM of UV PL peak with the concentration of KOH. (b) Visible PL spectrum fitted with Gaussian functions for the ZnO NPs synthesized for 40 days with 0.75 M KOH.

For 0.5 M of KOH, the visible emissions appeared at about 418 nm, 448 nm, 491 nm, 540 nm, and 582 nm. Intensities of these peaks decrease from lower wavelength to higher wavelength. For the other two samples, the visible emission band becomes clear with the center at ~550 nm. For a systematic detail study, this peak is fitted with Gaussian line shapes. Peak positions of the fitted peaks are extracted from free-parameter fittings. The visible PL spectrum along with Gaussian function fitted spectra for ZnO NPs prepared using 0.75 M of KOH is shown in Figure 5(b). Three Gaussian line shapes centered at ~491 nm, ~540 nm, and ~595 nm are used to fit the visible PL emission spectra. For 1.0 M of KOH, the shape of visible emission spectra is almost the same as that of 0.75 M of KOH but with much-reduced intensity.

The origin of PL emission centered at ~418 nm is due to the singly ionized oxygen vacancy in ZnO or oxygen antisite defect (O_{Zn}) [5]. The emission peaks at ~448 nm and ~491 nm are due to mainly the electron transitions from shallow donor levels (zinc interstitial) to the top of the valance band [5]. The PL emission peak at ~540 nm originated due to singly ionized oxygen vacancy [14]. However, the broad peak at ~576 nm is unlikely to be related to intrinsic defects. Since the peak is broad, it is likely to be related to disorder at the surface of the NPs. Surface atoms in the smaller ZnO NPs are expected to experience disorder and strain. As mentioned above, the visible emission is much reduced for ZnO NPs with 1.0 M of KOH. The reduction of visible PL emission intensity is also indicative of the reduction of various defects in ZnO NPs [5,7,14]. This is consistence with the UV PL emission data (reduction of FWHM with an increase in KOH concentration) and again establishes that the use of higher KOH concentration resulted in the synthesis of good quality ZnO NPs. However, this does not guarantee that the crystal quality will improve linearly with KOH concentration as the pH of the solution changes with the concentration of KOH.

The normalized PL emission spectra of ZnO NPs synthesized with 1.0 M of KOH and different times of synthesis (10 days – 60 days) are shown in Figure 6. Two emission bands are clearly seen in all the samples. The overall intensity of PL spectrum corresponding to the sample for 10 days of preparation is found to be much smaller compared to the intensities of other samples as evident from the scattering of the data points. These emission spectra are similar to that of ZnO NPs synthesized with 1.0 M of KOH for 40 days [filled triangles up in Figure 5(a)]. The observed difference in these spectra is the significant change in the intensity of visible emission for different times of synthesis. Although nearly comparable visible intensity is seen for the ZnO NPs synthesized for 20 days and 40 days, a systematic reduction of visible PL intensity is found with an increase in the time of synthesis. Such reduction of intensity is due to the reduction of various defect states (discussed above) in ZnO NPs. Because of the large time of synthesis, the NPs get sufficient time to repair the defect states within it leading to a reduction in the intensity of visible PL emission [5]. A reduction of the intensity of visible PL emission with the same intensity of UV emission for different samples is equivalent to the enhancement of UV emission. This can be observable if we plot the variation of the ratio of the intensity of UV emission (I_{UV}) and intensity of visible emission (I_{Vis}). The variation of I_{UV}/I_{Vis} is shown in Figure 7. Although a lot of scattering in the data points exists, an increase in I_{UV}/I_{Vis} with the time of preparation is seen. This indicates an enhancement of UV PL emission with the increase in time of synthesis. Nearly a 2-*fold* enhancement of the intensity of UV PL emission was recorded. Thus it is possible to enhance the UV emission of ZnO NPs by increasing the time of synthesis when synthesized at room temperature. Also, enhancement of UV PL emission of ZnO NPs is possible by changing the concentration of KOH [Figure 5(a)].

states may get more populated compared to the higher excitation energies. As a result, more intense visible PL emission is possible for excitation energy close (but greater) to the bandgap energy of ZnO.
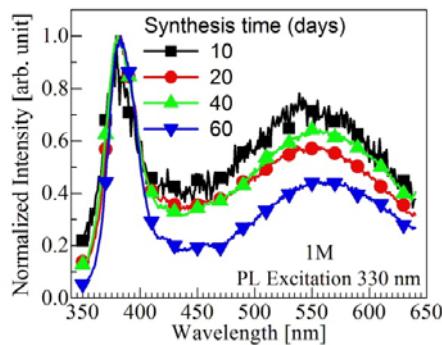

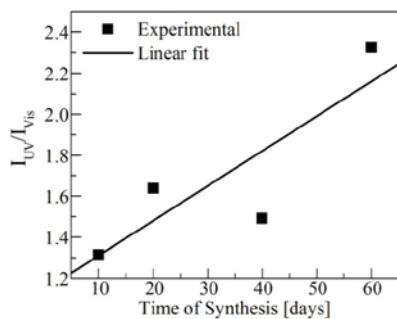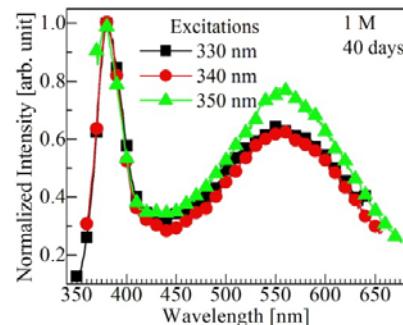Figure 6: PL spectra of ZnO NPs synthesized using 1.0 M of KOH for different days of synthesis duration.

Figure 7: Variation of the intensity ratio of UV to visible emissions of ZnO NPs with the time of synthesis. The solid line is the linear fit to the experimental data points.

As mentioned above (in Experiments), we have also carried out PL measurements of the ZnO NPs synthesized with 1.0 M of KOH for a synthesis time of 40 days by varying the excitation energy (or wavelength). The PL spectra for excitation wavelengths of 330 nm (3.76 eV), 340 nm (3.65 eV), and 350 nm (3.54 eV) are shown in Figure 8. Similar to the previous PL spectra of ZnO NPs [Figures 5(a) and 6] here also we get UV and visible emission bands. For 330 nm and 340 nm of excitations, the PL spectra are almost the same. However, for 350 nm of excitation, the intensity of visible PL emission is more than that of the other excitations. Such a small change in the visible PL emission can be understood in terms of the excitation energies used. The excitation energies used are always greater than the bandgap energy of the ZnO NPs (3.44 eV, estimated using EMA model for the average size of ZnO NP of 11.5 nm measured using XRD data). Such excitation energies always populate the electrons from the top of the valance band to the bottom of the conduction band and the defect states below the conduction band of ZnO NPs. As a result, a similar PL emission spectrum is expected from the ZnO NPs. When the excitation energy approaches the bandgap energy, defects

Figure 8: PL spectra of ZnO NPs synthesized for 40 days using 1 M of KOH for different excitations.

4. Conclusion

ZnO NPs of average crystallite size of ~11.5 nm have been synthesized at room temperature following the co-precipitation method by either varying the concentration of KOH or the time of synthesis. The size of NPs has not been changed with the change in KOH concentration or time of preparation as there is no sufficient heat energy required to grow the particles. However, the increase in the concentration of KOH or time of preparation has been found to increase the quality of the ZnO crystallites. Improvement of crystallite quality has resulted in a significant reduction in the intensity of defect-mediated visible PL emission band. In other words, an enhancement of the intensity of UV PL emission band with an increase in the concentration of KOH or time of synthesis is possible. In the present study, the enhancement of UV PL band is about 2-*fold*. Such large enhancement can be utilized for the fabrication of optoelectronic devices based on ZnO NPs synthesized at room temperature.

References

[1] A Meldrum, R F Jr Haglund, L A Boatner, and C W White, Nanocomposite Materials Formed by Ion Implantation, Adv. Mater., 13, 1431 (2001)

[2] P K Kuiri, H P Lenka, J Ghatak, G Sahu, B Joseph, and D P Mahapatra, Formation and growth of SnO2 nanoparticles in silica glass by Sn implantation and annealing, J. Appl. Phys., 102, 024315 (2007)

[3] X Wang, J B Xu, W Y Cheung, J An, and N Ke, Aggregation-based growth and magnetic properties of inhomogeneous Cu-doped ZnO nanocrystals, Appl. Phys. Lett., 90, 212502 (2007)

[4] D C Reynold, D C Look, BJogai, and H Morkoc, Similarities in the bandedge and deep-centre photoluminescence mechanisms of ZnO and GaN, Solid State Commun., 101, 643 (1997)

[5] S Pramanik, T Ghosh, M Ghosh, S C De, and P K Kuiri, Synthesis and time dependent growth of ZnO nanoparticles using solution route, and the defect-free luminescence, Adv. Sci. Eng. Med. 9, 414 (2017)

[6] H Zeng, G Duan, Y Li, S Yang, X Xu, and W Cai, Blue Luminescence of ZnO Nanoparticles Based on Non-Equilibrium Processes: Defect Origins and Emission Controls, Adv.Funct. Mater. 20, 561 (2010)

[7] S Pramanik, T Ghosh, M Ghosh, S C De, and P K Kuiri, Quenching of blue–green luminescence of ZnO nanoparticles obtained by solution route with different precursor concentration, J. Nanoele. Optoele. 13,, 428 (2018)

[8] P K Kuiri and S Pramanik,Large enhancement of UV luminescence emission of ZnO nanoparticles by coupling excitons with Ag surface plasmons J. Appl. Phys. 123, 154302 (2018)

[9] M Ghosh and A K Raychaudhuri, Shape transition in ZnO nanostructures and its effect on blue-green photoluminescence, Nanotechnology, 19, 445704, (2008)

[10] S Mukherjee, S Pramanik, S Das, S Chakraborty, R Nath, and P K Kuiri, Structural, optical, and electrical properties of $Zn_{1-x}Al_xO$ nanoparticles near the Al solubility limit, J. Alloys Comp. 814, 152015 (2020)

[11] S Mukherjee, S Pramanik, S Das, S Chakraborty, S Mondal, T Ghosh, R Nath, and P K Kuiri, Oriented attachment induced morphology modulation of ZnO nanoparticles at low temperature using KOH as a morphology controller, New J. Chem., 45, 17009 (2021)

[12] S Mukherjee, S Pramanik, S Das, G Bhattacharjee, S Mondal, T Ghosh,, A Chattopadhyay, D Sao, R Nath, and P K Kuiri, Control synthesis of low aspect ratio Zn1-xAgxO nanorods using low temperature solution route: Evidence of Ag concentration dependent shape transition, Mat. Res. Bull. 148, 111673 (2022)

[13] F Liu, Y H Leung, A B Djurisic, A M Ching Ng, and W K Chan,Native Defects in ZnO: Effect on Dye Adsorption and Photocatalytic Degradation,J. Phys. Chem. C 117, 12218 (2013).

[14] S Pramanik, S Mondal, A C Mandal, S Mukherjee, S Das, T Ghosh, R Nath, M Ghosh, and P K Kuiri, Role of oxygen vacancies on the green photoluminescence of microwave-assisted grown ZnO nanorods, J. Alloys Comp. 849, 156684 (2020)

[15] P K Sharma, A C Pandey, G Zolnierkiewicz, N Guskos, C Rudowicz, J. Appl. Phys. 106 , 094314 (2009).

[16] L Brus, electronic wave functions in semiconductor clusters: Experiments and theory, J Phys Chem, 90, 2555 (1986)

[17] A A Mosquera et al., Exciton and core-level electron confinement effects in transparent ZnO thin films, Scientif Rep. 3, 1714 (2013)

[18] P K Kuiri and D P Mahapatra, Effects of annealing atmosphere on ZnO– ions-implanted silica glass: synthesis of Zn and ZnO nanoparticles, J. Phys. D: Appl. Phys. 43, 395404 (2010)

[19] B L Caetano et al., Unified ZnO Q-dot growth mechanism from simultaneous UV-Vis and EXAFS monitoring of sol-gel reaction induced by different alkali base, Opt. Mater. 61, 92-97 (2016)

[20] H L Cao et al., Shape and size controlled synthesis of nanometre ZnO from a simple solution route at room temperature, Nanotechnology. 17, 3632 (2006)

[21] M A M Moazzen et al., Change in the morphology of ZnO nanoparticles upon changing the reactant concentration, Appl. Nanosci. 3, 295-302 (2013)

[22] B Ludi and M Niederberger, Zinc oxide nanoparticles: chemical mechanisms and classical and non-classical crystallization, Dalton. Trans, 42, 12554-12568 (2013)